Optics & Laser Technology 140 (2021) 107063

Contents lists available at ScienceDirect

Optics and Laser Technology

journal homepage: www.elsevier.com/locate/optlastec

Full length article

Wavelength and intensity based lossy mode resonance breathing sensor

D. Bohorquez [a], I. Del Villar [a,b,*], J.M. Corres [a,b], I.R. Matias [a,b]

[a] Department of Electrical and Electronic Engineering, Public University of Navarra, 31006 Pamplona, Spain
[b] Institute of Smart Cities, Public University of Navarra, Pamplona 31006, Spain

ARTICLE INFO

Keywords:
Lossy mode resonances
Photonic sensors
Thin-films
Optical planar waveguides
Sputtering technique

ABSTRACT

Copper oxide (CuO) allows the generation of lossy mode resonance (LMR) in a wide wavelength range of the optical spectrum, both in the visible and the near-infrared (NIR). For this, it is necessary to use a configuration based on the lateral incidence of light on the edge of a planar waveguide structure. On the other hand, the use of additional coatings of tin oxide (SnO_2) and agarose allows an increase in the sensitivity of the sensor, in response to the breathing monitoring. The sensors were characterized, both in intensity and wavelength. In both cases their behavior depends on the position of the LMR in the optical spectrum. Therefore, it is convenient to extract the design rules that allow an optimal behavior of the sensor. In this sense, sensors located in the NIR presented a better behavior in terms of sensitivity and quality of the signal. In addition, the devices were tested in different conditions: repetitive tests at different distances, oral and nasal breathing, and breathing after doing physical exercise.

1. Introduction

Scientific research in biology, genetics and medicine have focused on improving the quality of life of people through the study, diagnosis and monitoring of physiological variables. One of the variables that arouses the most interest is breathing [1].

Through breathing, it is possible to evaluate the physiological state of the human body by recording some of its characteristic parameters, such as respiratory rate [3]. The respiratory rate is the number of breaths taken in a certain period. This physiological parameter, together with heart rate and blood pressure, are used to estimate the basic health status of patients [4]. Abnormalities in respiratory rate and breathing patterns are predictors of disorders such as cardiac arrest, lung disease (such as pneumonia), and sleep apnea syndrome (SAS), among others [2-6].

Several methods have been implemented for the breathing monitoring, such as the use of precision biomedical instruments based on sound, airflow, the use of wireless communication technologies, data analysis and sensors [4-7]. In the field of sensors, there exist several types, such as temperature sensors (which detect the temperature variations between inhaled and exhaled airflow), pressure sensors (which detect the expansion and constriction of the chest or the airflow from the nose), and acoustic sensors (which monitor breathing based on sound) [2-4]. There are also electronic breathing sensors based on different approaches such as piezo-electric films, dry textile electrodes and flexible capacitive electrodes [7]. However, electronic sensors are sometimes not stable and are sensitive to electromagnetic interference, which inhibits their application in magnetic resonance imaging (MRI) and in oncological treatments requiring the administration of radiation or high electric or magnetic fields [3-8], for example.

Other sensors that have been used to monitor respiration are optical fiber sensors and these possess certain characteristics, such immunity to electromagnetic interference, lightweight, small size, high sensitivity and large bandwidth [8,9].

Optical fiber sensors can be classified in three main groups: interferometers, grating based sensors and sensors based on resonances generated by a thin-film [10]. Within the latter group, one can find two main groups: surface plasmon resonance (SPR) [11] and lossy mode resonance (LMR) based sensors [12]. However, though both phenomena are generated under the presence of a thin-film, the conditions for excitation of the resonance are quite different: SPRs are obtained when the real part of the thin film permittivity is negative and higher in magnitude than both its own imaginary part and the permittivity of the material surrounding the thin film, whereas LMRs occur when the real part of the thin film permittivity is positive and higher in magnitude than both its own imaginary part and the material surrounding the thin film [12,13]. These conditions are mathematically expressed in Table 1 under the assumption that the outer medium presents a lower refractive

* Corresponding author at: Department of Electrical and Electronic Engineering, Public University of Navarra, 31006 Pamplona, Spain.
E-mail address: ignacio.delvillar@unavarra.es (I. Del Villar).

https://doi.org/10.1016/j.optlastec.2021.107063
Received 18 November 2020; Received in revised form 10 February 2021; Accepted 5 March 2021
Available online 21 March 2021

Table 1
Conditions for generation of SPRs and LMRs (ε_1, ε_2, n_1, n_2, k_1 and k_2 represent the permittivity, refractive index and extinction coefficient for the substrate (1) and the thin film (2) respectively).

Type of resonance	Conditions (ε)	Conditions (n,k)
SPR	$\varepsilon_2^{'} < 0$ $\lvert\varepsilon_2^{'}\rvert > \lvert\varepsilon_2^{''}\rvert$ $\lvert\varepsilon_2^{'}\rvert > \lvert\varepsilon_1^{'}\rvert$	$k_2 > (\sqrt{2}+1)n_2$ $k_2^2 - n_2^2 > n_1^2$
LMR	$\varepsilon_2^{'} > 0$ $\lvert\varepsilon_2^{'}\rvert > \lvert\varepsilon_2^{''}\rvert$ $\lvert\varepsilon_2^{'}\rvert > \lvert\varepsilon_1^{'}\rvert$	$k_2 < (\sqrt{2}-1)n_2$ $n_2^2 - k_2^2 > n_1^2$

index than the substrate. The equations for the refractive index and the extinction coefficient clearly show why SPRs are typically obtained with metallic thin-films whereas LMRs are generated with metallic oxides and polymers [12]. In addition, unlike SPRs, generated only at TM polarization, LMR based sensors have the ability to operate with resonances generated at both TE and TM polarized light [14] and are typically excited with angles of incidence approaching 90° (grazing incidence) [12]. This explains its success in the domain of optical fiber sensors, where they have been used to detect humidity [15], gases [16] and antibodies [17].

Regarding the structures that are used for obtaining LMR-based sensors, D-shaped fiber is preferred than cylindrical geometry based structures such as multimode fiber and tapered single mode fiber [12], because it permits to separate the TM and TE components of the optical spectrum [18,19]. However, D-shaped fiber is not easy to obtain or handle. For this reason, planar waveguide structures (slides and coverslips) have been used in this work with lateral incidence of light on the edge of the waveguide [20]. Unlike D-shaped fiber, these structures are easier to use and do not limit the range of operation of the optical spectrum, and at the same time they permit to separate the TM and TE components. Moreover, the waveguide can be coated on both sides, which makes it possible to obtain a sensor that can measure more than one parameter at the same time [21].

Taking into account the advantages of using planar waveguide structures in the manufacture of LMR sensors, in this work an LMR based sensor has been developed for breathing monitoring. The basis for the development of the sensor was the utilization of a CuO coating, which was used in a previous work for generating LMRs both in the visible and NIR wavelength for humidity sensing [22]. Here, taking into account that a shorter response time is required in breathing monitoring, one step forward was followed by comparing the performance of the device in wavelength and intensity based configurations. Considering the results obtained in both configurations, it is possible to extract some conclusions towards optimization of the performance of the final device, whose behavior also depends on the deposition or not of a final agarose layer.

2. Methods

2.1. Sensor design

The experimental setup of the breathing monitoring sensor structure is shown in Fig. 1. It consists of a light source (ASBN-W halogen tungsten broadband from Spectral Products), two multimode optical fibers from Ocean Optics (200/225 μm of core/cladding diameter) and two USB2000 FLG and NIRQUEST spectrometers (from Ocean Optics Inc.), for the breathing monitoring in both visible and infrared regions. By replacing the spectrometers with a photodiode with a wide spectral range (200–1100 nm), model PD300-UV P / N7Z02413 from Ophir Photonic, the optical signal can be obtained in intensity, instead of in wavelength. The fundamental objective of this second intensity measure is its potential use in an industrial application.

The light source is connected to one end of the multimode fiber and the other end is positioned in front of one edge of the planar waveguide (coverslip). The light that comes out of the waveguide is coupled to another fiber which, in turn, is connected to either the USB2000 FLG and NIRQUEST spectrometers or to the photodiode, depending on whether the wavelength or intensity is to be measured, respectively. Two sensors were manufactured, S1 and S2. In S1, the coverslip was supported on a base of polymethyl methacrylate (PMMA) and covered with two thin films of metal oxide: first with copper oxide (CuO) to generate the LMR and, subsequently, with tin oxide (SnO_2) to avoid the degradation of the first film and to make the surface sensitive to humidity from the breath. In addition, the tin oxide target was oxygen depleted and strictly

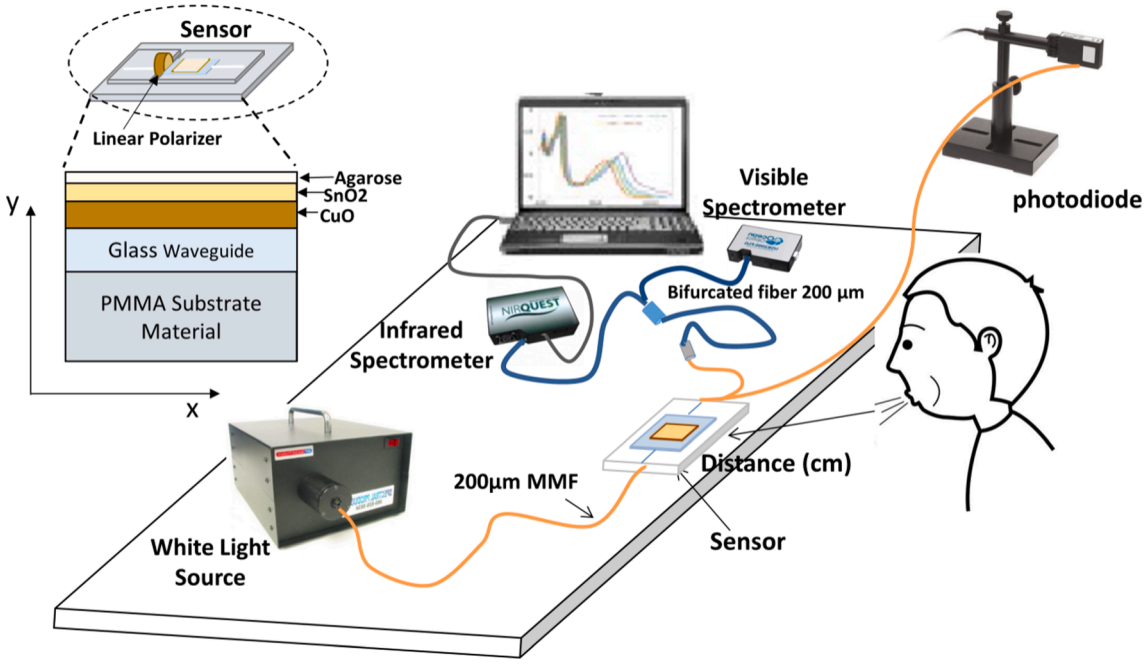

Fig. 1. Experimental setup for breathing monitoring in real-time. The proposed setup allows obtaining the sensor response in wavelength, using a visible and NIR spectrometer, or in intensity, using a photodiode.

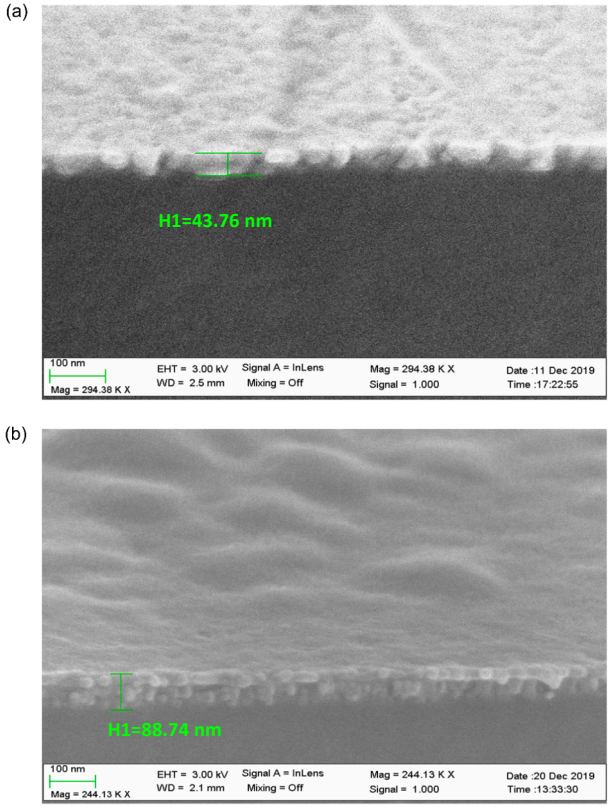

Fig. 2. Scanning electron microscope (SEM) image obtained for the characterization of the thickness of each deposited coating for the sensors: (a) S1 (CuO + SnO_2); (b) S2 (CuO + SnO_2 + Agarose 0.5% w/v).

speaking is SnO_{2-x}, though for the sake of simplicity it will be referred throughout the manuscript as SnO_2.

Both CuO and SnO_2 were deposited by using a DC sputtering machine (K675XD from Quorum Technologies, Ltd.). The parameters used in the deposition of CuO were 6×10^{-2} mbar argon partial pressure, 75 mA of current intensity and deposition time 6 min. Regarding SnO_2, the parameters were 7×10^{-2} argon partial pressure, 90 mA of current intensity and deposition time 40 s. The evolution of the spectrum during the deposition of the thin-films was monitored with Spectra Suite program (Ocean Optics Inc.) and the experimental configuration implemented is shown in Fig. 1.

The deposition was implemented so that the TM mode was located in the visible region and the TE mode in the infrared, in order to be able to compare the performance of the sensors in both spectral ranges. This capability to monitor an LMR in both the visible and the infrared regions is due to the fact that the refractive index and extinction coefficients of CuO meet the conditions for generation of LMRs in all this wavelength range: n ranges from 2.2 to 2.3 whereas k ranges from 0 to 1 [23].

S2 consists of the same structure as S1 but presents an additional agarose layer at 0.5% w/v. For the preparation of the agarose, the method described by Arregui et *al.* was followed [24] while, for its deposition, the spin coating technique was applied, (WS-650SZ-6NPP/LITE from Laurell was used at 700 rpm 3 min).

The thickness of the coatings deposited on sensors S1 and S2 was characterized using a field emission scanning electron microscope (model UltraPlus FESEM from Carl Zeiss Inc.) with an in-lens detector at 3 kV and an aperture diameter of 30 μm. Fig. 2 shows a microscopic image of these coatings. S1 has a coating with a total thickness of 44 nm (Fig. 2a), where the SnO_2 coating (5–10 nm) cannot be distinguished due to its thinness and because both CuO and SnO_2 are metallic oxides. In S2, the SnO_2 layer cannot be distinguished either. However, now there are two regions for a total thickness of 89 nm: an upper region, corresponding to agarose, and a lower region corresponding to the set of SnO_2 together with CuO (Fig. 2b).

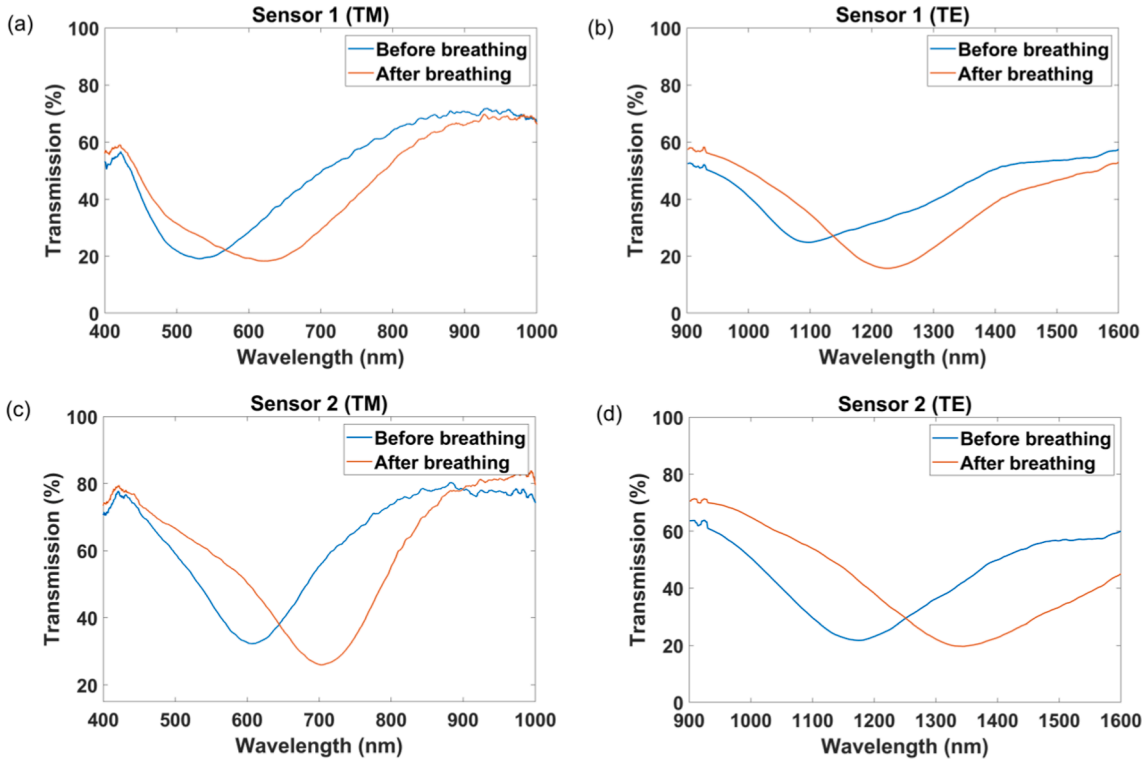

Fig. 3. Characterization of the resonances and responses of S1 and S2 to the monitoring of normal breathing at a distance of 2 cm: (a) optical spectrum of S1, visible region, TM; (b) optical spectrum of S1, NIR region, TE; (c) optical spectrum of S2, visible region, TM; (d) optical spectrum of S2, NIR region, TE.

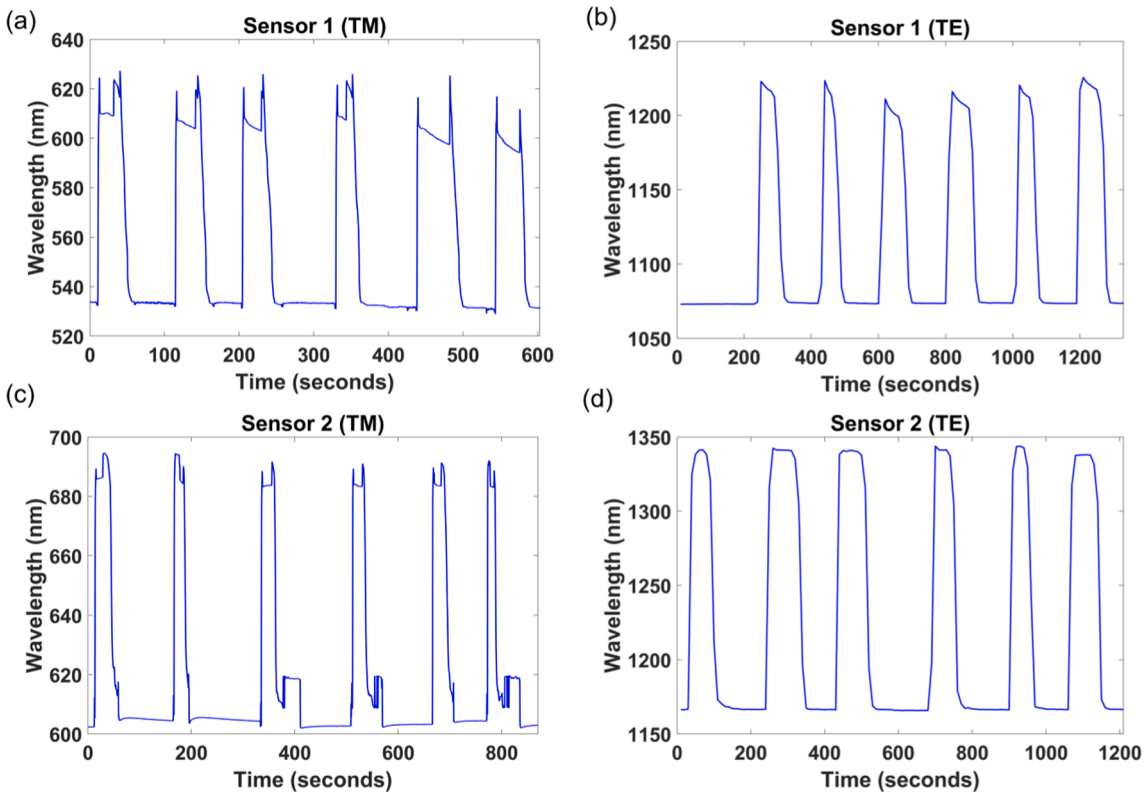

Fig. 4. S1 and S2 wavelength responses to breathing: (a) S1, visible region, TM; (b) S1, NIR region, TE; (c) S2, visible region, TM; (d) S2, NIR region, TE.

2.2. Breathing monitoring

In order to evaluate the response of the S1 and S2 sensors to breathing, two types of tests were performed. The first one consisted of monitoring the breathing as a wavelength shift in the central LMR peak for both the visible region (using the USB2000 FLG) and the infrared region (using the NIRQUEST), whereas the second one consisted of monitoring the breathing intensity as a function of the output optical power response of a Photodiode PD300-UV P/N7Z02413 (Ophir Photonic). In view of the faster response time of the second setup, S1 and S2 sensors were placed at different distances from an individual's mouth and were subjected to oral breathing tests at different distances, whereas the best sensor was also tested after doing physical exercise and for nasal breathing. The response time of the sensors was also analyzed in detail.

3. Results and discussion

3.1. Characterization of the sensor

In Fig. 3a and 3b it is possible to see the spectral bands (TE and TM polarization) corresponding to the LMR peaks obtained after the manufacture of S1. Likewise, in Fig. 3c and 3d, it is possible to observe the spectral bands corresponding to the LMR peaks obtained after the construction of S2, where an additional layer of agarose was deposited. It is important to indicate that the LMR at TE polarization is located in both sensors in the infrared, whereas the LMR at TM polarization is located in the visible spectral region. This is the typical behavior in LMR based sensors: the LMR at TE polarization is located at longer wavelengths because the cutoff wavelength for TE modes is located at longer wavelength than for TM modes.

3.2. Evaluation of the sensor response to breathing

In Fig. 3 it is also possible to observe, for all the cases analyzed, the wavelength shift generated during the breathing cycle (inhalation and exhalation), when sensors S1 and S2 were located at a distance of 2 cm from the mouth of a subject. A wavelength change in the LMR peaks is observed in both sensors when the subject exhales air. S1 showed a wavelength shift of 94 and 133 nm in the visible region and NIR respectively, which demonstrates that the wavelength shift is greater in the NIR region according to what has been observed in the literature [17]. This behavior was also observed in S2, which presented a wavelength shift of 95 and 167 nm at TM and TE polarization, respectively. These results indicate that the presence of the agarose layer induces a higher wavelength shift in the infrared compared to sensor S1, while this effect is diminished in the visible region.

In addition, it must be pointed out that in the literature the figure of merit (FOM) is rather used for assessing the performance of an optical sensor [10], and the FOM is typically the ratio between the sensitivity and the full width at half minimum (FWHm). If the FWHm is evaluated, the results show that this parameter is lower in the visible region (TM) than in the NIR region (TE): 195 nm and 229 nm at TM and TE respectively for S1. This indicates that the FOM is quite similar in for both TM and TE LMRs: the improvement in terms of wavelength shift in the infrared is balanced by the reduction of the FWHm in the visible region.

Fig. 4 shows the wavelength response of sensors S1 and S2 for 6 consecutive inhalation/exhalation cycles. As shown in Fig. 3, after each breathing cycle, the LMR moves towards longer wavelengths. The lower part of the wavelength response to breath, corresponding to shorter wavelengths, corresponds to the state of inhalation, while the upper part indicates exhalation. It should be noted that the measurements were taken with a high sampling time because the spectrometer used required an increase in this parameter to achieve a sufficient optical intensity in the wavelength range analyzed. This implies that it is convenient to use an intensity scheme where the sampling time is much shorter and the response of the sensor can be better characterized, in terms of rise and fall times.

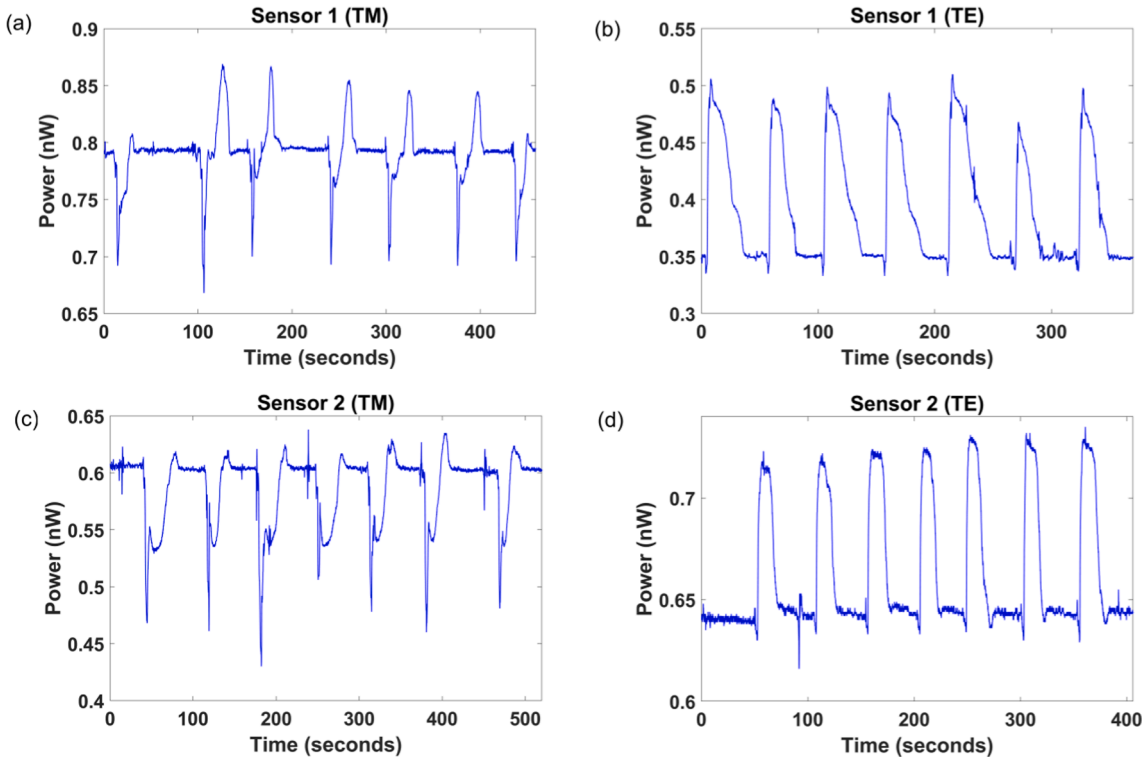

Fig. 5. S1 and S2 intensity responses to breathing: (a) S1, visible region, TM; (b) S1, NIR region, TE; (c) S2, visible region, TM; (d) S2, NIR region, TE.

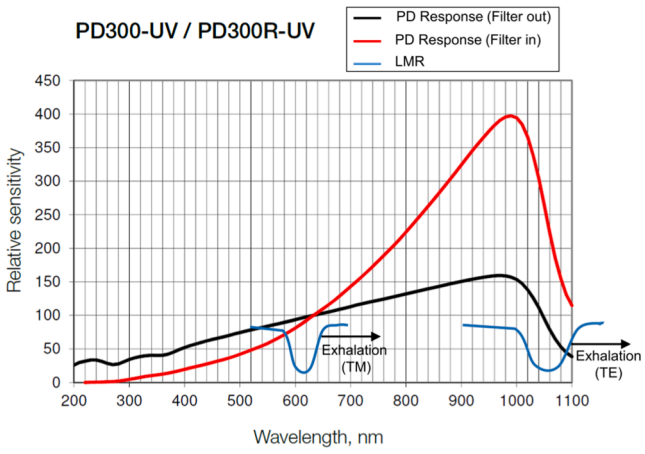

Fig. 6. Spectral response of the photodiode PD300-UV P/N7Z02413 (Ophir Photonics) with and without a filter. The positioning of the LMR in the wavelength determines whether the detected power by the photodetector changes in one direction or another and also the intensity of this change.

Fig. 5 shows the signals corresponding to 7 consecutive inhalation/exhalation cycles applied to S1 and S2 when located at a distance of 2 cm from a subject's mouth (this time the measurement is in intensity). It can be seen that, during the exhalation process, in both S1 and S2 the power received by the detector decreases in the visible region considering the TM polarization (Fig. 5a and 5c) and it presents an irregular evolution of the signal (in some cases the signal exceeds the base line before the initial state is recovered). Therefore, focus will be centered on the TE polarization (Fig. 5b and 5d), where the change of the signal is higher and the behavior is less irregular.

Fig. 5b and 5d show the change of power generated in S1 and S2 in the NIR region at TE polarization (the base line represents the inhalation and the upper peaks the exhalation for each breathing cycle). In S1, the output optical power increases from 0.353 to 0.491 nW with an average rise time of 2.14 s and an average fall time of 21.4 s with a standard deviation (SD) of 0.23 and 5.03 s, respectively. In the case of S2, the output optical power increases from 0.644 to 0.726 nW at an average rise time of 1.63 s and an average fall time of 7.55 s with an SD of 0.16 and 2.42, respectively. It should be noted that sensor S2 recovers faster than S1.

The different intensity behavior of TE and TM sensors is explained by Fig. 6, where it is shown that the spectral response of the photodiode used in the experiments has an upward curve below 1000 nm and a downward curve above 1000 nm. This is the reason why when the LMR is located in the visible region (TM polarization) the output optical signal intensity decreases when air is exhaled; the LMR absorbs power in the region where the photodiode captures more energy, hence the output optical power decreases. On the other hand, for the LMR obtained in TE polarization (approximately 1100 nm), the exhalation of the air causes the LMR to move to a region where the photodiode captures less energy and, therefore, the output optical power increases.

Fig. 6 also shows two photodiode curves, with and without a filter. In the experiments, the unfiltered photodiode was used, where the signal drop is more abrupt at longer wavelengths than at shorter wavelengths. This explains why the LMR obtained with TE polarization exhibits a better response. In view of these results, the best design is to position the LMR in a region where the photodiode relative sensitivity response signal as a function of wavelength has a more pronounced slope, in order to obtain a greater dynamic range.

Once this has been explained, it seems clear that the best option is to monitor the LMR located in the infrared, i.e. for TE polarization. So, from now on, we will work on this case.

Fig. 7 shows the results obtained in the monitoring of the breathing of a subject at rest in real time, when sensors S1 and S2 in TE were placed at different distances: 2, 4, 6, 8, 10 and 12 cm from the subject's mouth. It is observed that both S1 and S2 are capable of monitoring the breathing at different distances (Fig. 7a and 7c), responding adequately to each inhalation (base line) and exhalation process (peak) for each breathing cycle. Fig. 7b and 7d show the relationship that exists between

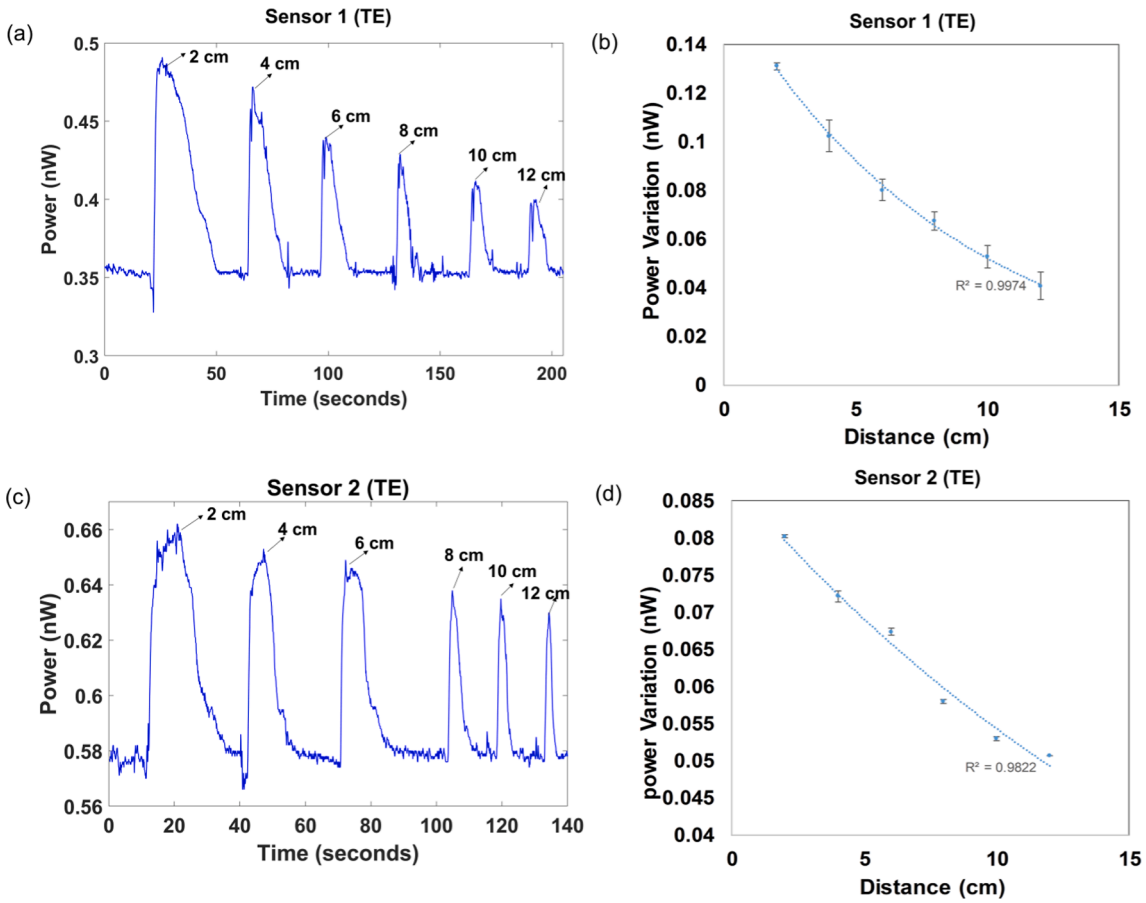

Fig. 7. Intensity response to breathing monitoring at different distances: (a) sensor S1; (c) sensor S2. Relationship between the different distances at which the sensors S1 and S2 are placed and the output optical power observed: (c) sensor S1; (d) sensor S2.

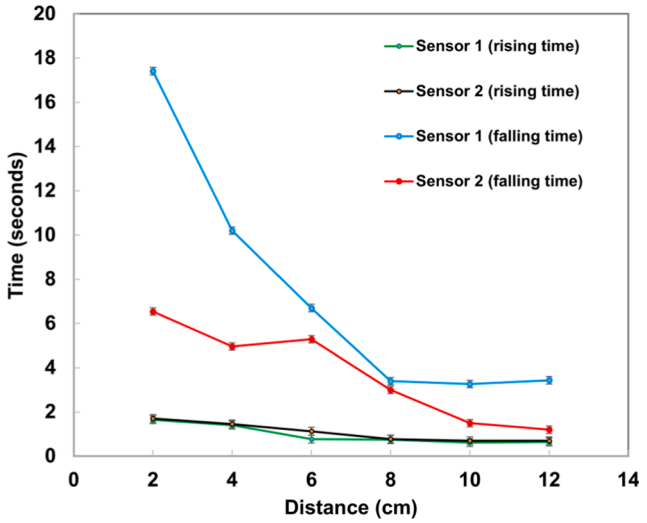

Fig. 8. Response rise and fall times for sensors S1 and S2 in the monitoring of the breathing when placed at different distances.

the distances at which the sensors were located and the optical power obtained by the detector. It can be concluded that the signal decreases as the exposure distance increases from the sensor to the subject's mouth. This is explained by the fact that the power intensity is directly related to the position of the LMR in the optical spectrum, as explained before. Therefore, the decrease of the power variation is due to a smaller shift of the LMR, because the thin film of agarose or tin oxide captures less water molecules. As a result, the effective refractive index is modified to a lesser extent.

Fig. 8 shows the values corresponding to the rise and fall response times of the sensors S1 and S2 in the monitoring of the breathing when placed at different distances. It is evident that, in both sensors, both the rise and the fall times decrease as the exposure distance of the sensor to the subject's mouth increases. S1 has a response rise time between 1.67 and 0.65 s and a fall time between 17.4 and 3.44 s. S2 has a rise time from 1.71 to 0.7 s and a fall time from 6.4 to 1.2 s, respectively for distances between 2 and 12 cm. Hence, it can be concluded that both sensors have a similar rise time but, in the case of the fall time, S2 responds in a shorter time than S1, i.e. it recovers faster. Indeed, according to the normal human breathing rate, between 6 and 30 breaths per minute, it presents adequate response times for human breathing at distances 10 and 12 cm from the sensor [25].

Fig. 9 shows an exhalation/inhalation cycle for both S1 and S2 sensors at a distance of 2 and 12 cm from a subject's mouth in the exhalation (rise) and inhalation (fall) phases for each breathing cycle. In Fig. 9a it is observed that sensor S1, at a distance of 2 cm, shows a rise time of 1.65 s and a fall time of 17.41 s, whereas it shows a rise time of 0.65 s and a fall time of 3.44 s when located at 12 cm (Fig. 9b). Regarding sensor S2, when located at a distance of 2 cm it shows a rise time of 1.71 s and a fall time of 6.54 s (Fig. 9c), whereas for a distance of 12 cm it showed a rise time of 0.7 s and a fall time of 1.2 s (Fig. 9d). These results confirm that sensor S2 has a better recovery time than sensor S1.

Regarding the comparison with other breath sensors, the response time of the interferometer based breath sensor of [8] was assessed by inducing humidity variations from 0 to 30% and analyzing the rise time and the recovery time, 0.4 and 0.5 s respectively [26], whereas the thin-

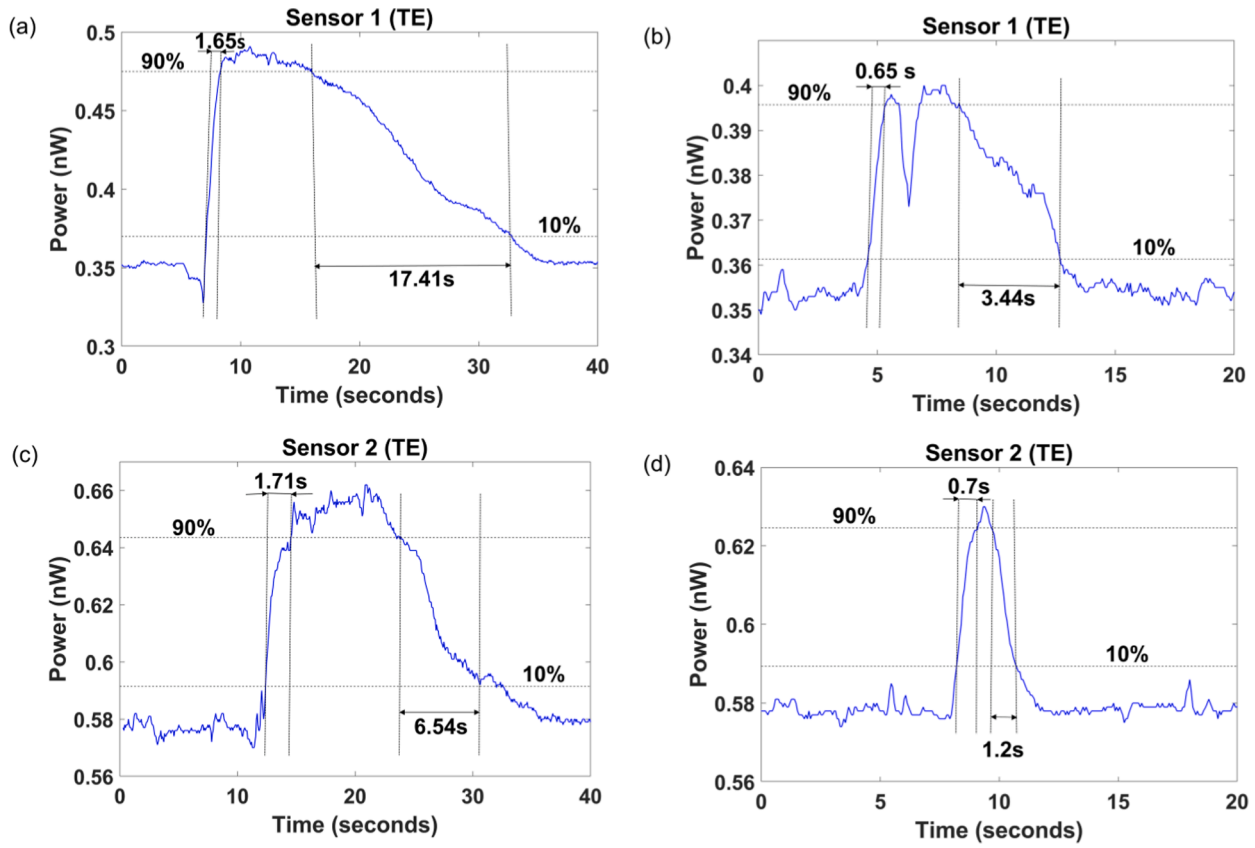

Fig. 9. Response and recovery times: (a) S1 at a distance of 2 cm; (b) S1 at a distance of 12 cm; (c) S2 at a distance of 2 cm; (b) S2 at a distance of 12 cm.

film based sensor analyzed in [3] shows 0.07 and 2.4 s rise and recovery time. Finally, regarding LMR based sensors, there is a precedent with thin-film coated multimode optical fiber where the response time is 0.1 s [27]. The difficulty with all these sensors is that no information on the distance is given, which is critical for an accurate comparison of the sensor performance.

Finally, Fig. 10 shows the real-time experimental response of S2 in TE polarization to breathing, both by breathing through the nose (nasal breathing) and after a physical activity, when the sensor was located at a distance of 2 cm from the subject. The nasal breathing is constant and the power reached by the detector experiences an output optical power change from 0.613 to 0.685 nW (Fig. 10a). However, the sensor response after exercise shows similar variations in power, from 0.619 to 0.696 nW, but the evolution of the signal is more irregular (Fig. 10b).

4. Conclusions

It has been demonstrated that deposition of coatings using different materials, such as semiconductor oxides and polymers, can be combined for the development and optimization of LMR-based sensors. In the specific case presented in this work, copper oxide (CuO) has been used in order to generate the LMRs in a wide spectrum, from the visible to the NIR. Due to this optical property, as well as to the use of lateral incidence of light on the edge of a coverslip for a glass slide, it has been possible to study the LMR in TE and TM mode in the same sensor and at very different wavelengths. This is something that is not possible neither with D-shaped fiber due to its narrow working wavelength range, nor with multimode fibers, where TE and TM cannot be separated.

Two cases have been analyzed with the aim of monitoring the human breathing: sensors where tin oxide has been deposited onto a CuO layer and sensors with an additional layer of agarose. It has been observed that the recovery time of the sensor with agarose is faster than the one without agarose, which indicates that this sensor is more appropriate for the monitoring of breathing.

In addition, the sensors were characterized in both wavelength and intensity, the latter case being demonstrated as a better option since the response time of the photodetector is faster than the spectrometer, allowing to follow the breathing signal more precisely.

Furthermore, it has become clear in the work that the response of the sensor depends on the alignment of the LMR with the spectral response of the photodetector used.

As proof of the performance of sensors in the infrared region, which show better sensitivity than those in the visible region, their response at different distances was studied. In this sense, the power received by the detector decreased as the exposure distance from the sensor to the subject's mouth was increased. Furthermore, taking into account that the best response time was obtained using the sensor with agarose, this sensor was analyzed for different breathing states: oral breathing, nasal breathing and post-exercise.

As a final remark, it has been demonstrated that the response in intensity is similar to that in wavelength for LMR based sensors, with the advantage that their response time is much faster. This is one more option for the use of this technology in industrial applications. In fact, intensity detection is much more economical as it allows the use of an LED source and photodetector instead of a broad-spectrum light source and a spectrometer.

CRediT authorship contribution statement

D. Bohorquez: Investigation, Writing - original draft. **I. Del Villar:** Writing - original draft, Writing - review & editing, Conceptualization, Supervision. **J.M. Corres:** Supervision, Methodology. **I.R. Matias:** Writing - review & editing, Supervision.

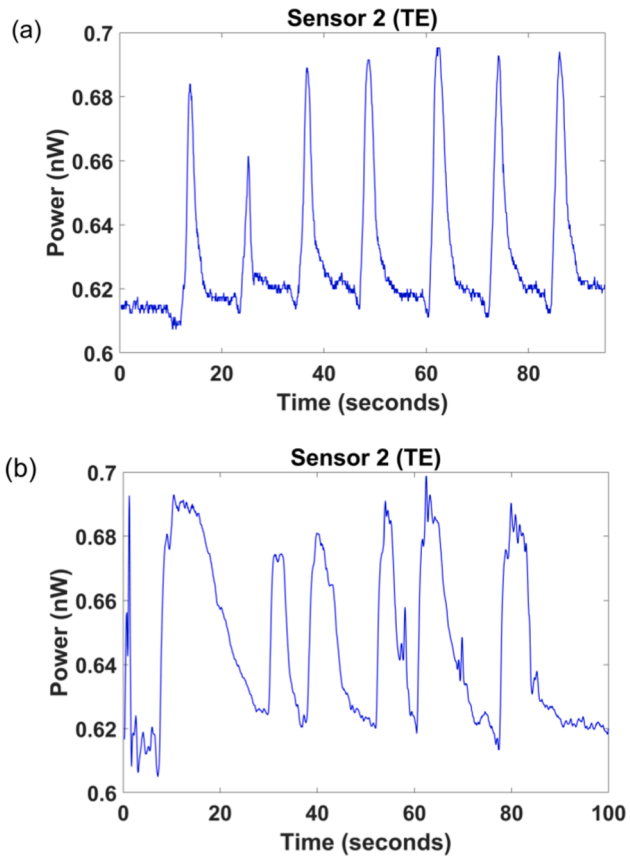

Fig. 10. Response of S2 to monitoring of the breathing (a) nasal; (b) after exercise.

Declaration of Competing Interest

The authors declare no conflicts of interest.

Acknowledgments

The authors would to acknowledge the partial support to the Agencia Estatal de Investigación (AEI) from the Spanish Ministry of Economy and Competitiveness (PID2019-106231RB-100 and PID2019-106070RB-100 research funds) and the pre-doctoral research grant of the Public University of Navarra.

References

[1] H. Hu, S. Sun, R. Lv, Y. Zhao, Design and experiment of an optical fiber micro bend sensor for respiration Monitoring, Sens. Act. A 251 (2016) 126–133.
[2] J. Dai, H. Zhao, X. Lin, S. Liu, Y. Liu, X. Liu, T. Fei, T. Zhang, Ultrafast response polyelectrolyte humidity sensor for respiration monitoring, ACS. Appl. Mater Interfaces 11 (2019) 6483–6490.
[3] B. Du, D. Yang, X. She, Y. Yuan, D. Mao, Y. Jiang, F. Lu, MoS2-based all-fiber humidity sensor for monitoring human breath with fast response and recovery, Sens. Act. B 251 (2017) 180–184.
[4] F. Güder, A. Ainla, J. Redston, B. Mosadegh, A. Glavan, T. Martin, G. Whitesides, Paper-Based Electrical Respiration Sensor, Angew. Chem. Int. Ed 55 (2016) 5727–5732.
[5] F. Yasuma, J. Hayano, Respiratory sinus arrhythmia: why does the heartbeat synchronize with respiratory rhythm? Chest 125 (2) (2004) 683–690.
[6] P. Várady, T. Micsik, S. Benedek, Z. Benyó, A novel method for the detection of apnea and hypopnea events in respiration signals, IEEE Trans. Biomed 49 (9) (2002) 936–942.
[7] A. Leal-Junior, C. Díaz, C. Leitão, M.J. Pontes, C. Marques, A. Frizera, Polymer optical fiber-based sensor for simultaneous measurement of breath and heart rate under dynamic movements, Opt. Las. Tech 109 (2019) 429–436.
[8] J. Mathew, Y. Semenova, G. Farrell, A miniature optical breathing sensor, Biomed. Opt. Express 3 (12) (2012) 3325–3331.
[9] Z. Chen, D. Lau, J. Teo, S. Ng, X. Yang, P. Kei, Simultaneous measurement of breathing rate and heart rate using a microbend multimode fiber optic sensor, J. Biomed. Opt. 19 (5) (2014), 057001.
[10] A. Urrutia, I. Del Villar, P. Zubiate, C.R. Zamarreño, A Comprehensive Review of Optical Fiber Refractometers: Toward a Standard Comparative Criterion, Laser Photon. Rev 13 (11) (2019), 1900094 1-32.
[11] H.E. Limodehi, F. Légaré, Fiber optic humidity sensor using water vapor condensation, Opt. Express 25 (2017) 15313–15321.
[12] I. Del Villar, F. Arregui, C.R. Zamarreño, J. Corres, C. Bariain, J. Goicoechea, C. Elosua, M. Hernaez, P. Rivero, A. Socorro, A. Urrutia, P. Sánchez, P. Zubiate, D. López, N. De Acha, J. Ascorbe, I.R. Matías, Optical sensors based on lossy-mode resonances, Sensors Actuat. B. Chem. 240 (2017) 174–185.
[13] F. Yang, J.R. Sambles, Determination of the optical permittivity and thickness of absorbing films using long range modes, J. Mod. Opt. 44 (6) (1997) 1155–1164.
[14] P. Sánchez, C. Zamarreño, M. Hernaez, I.R. Matias, F. Arregui, Optical fiber refractometers based on LossTy Mode Resonances by means of SnO2 sputtered coatings, Sens. Actuators. B 202 (2014) 154–159.
[15] C.R. Zamarreño, M. Hernaez, I. Del Villar, I.R. Matías, F. Arregui, Tunable humidity sensor based on ITO-coated optical fiber, Sens. Actuators. B 146 (1) (2010) 414–417.
[16] S. Usha, S. Mishra, B. Gupta, Fiber optic hydrogen sulfide gas sensors utilizing ZnO thin film/ZnO nanoparticles: A Comparison of surface plasmon resonance and lossy mode resonance, Sensors Actuat. B Chem. 218 (2015) 196–204.
[17] F. Chiavaioli, P. Zubiate, I. Del Villar, C. Zamarreño, A. Giannetti, S. Tombelli, C. Trono, F. Arregui, I.R. Matías, F. Baldini, Femtomolar Detection by Nanocoated Fiber Label-Free Biosensors, ACS Sens. 3 (5) (2018) 936–943.
[18] A. Andreev, B. Pantchev, P. Danesh, B. Zafirova, E. Karakoleva, E. Vlaikova, E. Alipieva, A refractometric sensor using index-sensitive mode resonance between single-mode fiber and thin film amorphous silicon waveguide, Sens. Actuators, B 106 (1) (2005) 484–488.
[19] P. Zubiate, C.R. Zamarreño, I. Del Villar, I.R. Matías, F. Arregui, High sensitive refractometers based on lossy mode resonances (LMRs) supported by ITO coated D-shaped optical fibers, Opt. Express 23 (6) (2015) 8045.
[20] O. Fuentes, J. Corres, I.R. Matías, I. Del Villar, Generation of Lossy Mode Resonances in Planar Waveguides Toward Development of Humidity Sensors, J. Lightwave Technol. 37 (10) (2019) 2300–2306.
[21] I. Rodriguez, I. Del Villar, O. Fuentes, J.M. Corres, I.R. Matías, Dually nanocoated planar waveguides towards multi-parameter sensing, Sci. Rep. 11 (2021) 3669.
[22] D.L. Bohorquez, I. Del Villar, J.M. Corres, I.R. Matias, Generation of lossy mode resonances in a broadband range with multilayer coated coverslips optimized for humidity sensing, Sensors Actuat. B. Chem. 235 (2020), 128795.
[23] O. Fuentes, J. Goicoechea, J.M. Corres, I. Del Villar, A. Ozcariz, I.R. Matías, Generation of lossy mode resonances with different Nanocoatings deposited on coverslips, Opt. Express 28 (1) (2020) 288–301.
[24] F. Arregui, Z. Ciaurriz, M. Oneca, I.R. Matías, Experimental study about hydrogels for the fabrication of optical fiber humidity sensors, Sensors Actuat. B. Chem. 96 (2003) 165–172.
[25] G. Benchetrit, Breathing pattern in humans: diversity and individuality, Respir. Physiol. 122 (2000) 123–129.
[26] J. Mathew, Y. Semenova, G. Farrell, Relative Humidity Sensor Based on an Agarose-Infiltrated Photonic Crystal Fiber Interferometer, IEEE J. Sel. Top. Quantum Electron. 18 (5) (2012) 1553–1559.
[27] P. Sanchez, C.R. Zamarreño, M. Hernaez, I.R. Matias, F.J. Arregui, Exhaled breath optical fiber sensor based on LMRs for respiration monitoring, Sensors, 2014 IEEE, Valencia, Spain, 2014, pp. 1142-1145.